Solvation Model Dependency of Helix-Coil Transition in Polyalanine

Yong Peng and Ulrich H. E. Hansmann
Department of Physics, Michigan Technological University, Houghton, Michigan 49931-1291 USA

ABSTRACT Helix-coil transitions in polyalanine molecules of length 10 are studied by multicanonical Monte Carlo simulations. The solvation effects are included by either a distance-dependent dielectric permittivity or by a term that is proportional to the solvent-accessible surface area of the peptide. We found a strong dependence of the characteristics of the helix-coil transition from the details of the solvation model.

INTRODUCTION

There has recently been a renewed interest in the conditions under which α-helices, a common structure in proteins, are formed or dissolved. It is well known that α-helices undergo a sharp transition toward a random coil state when the temperature is increased. The characteristics of this so-called helix-coil transition have been studied extensively (Poland and Scheraga, 1970), most recently in Kemp and Chen (1998) and Hansmann and Okamoto (1999). In Alves and Hansmann (2000, 2001) evidence was presented that the helix-coil transition in polyalanine exhibits a true thermodynamic phase transition when interactions between all atoms in the molecule are taken into account.

The latter results were obtained from gas-phase simulations of polyalanine. Although there is some experimental evidence (Hudgins et al., 1998) supporting the numerical results of these gas-phase simulations, the question remains how these results relate to the biologically more relevant case of solvated molecules. The first investigations of this question were described in Mitsutake and Okamoto (1999, 2000) where it was claimed that the transition temperature is lower in water than in vacuum. However, that investigation relies on a single representation of the protein-water interaction, and the dependence of their results on the details of the solvation term is not clear.

In this paper we have investigated how the characteristics of helix-coil transition change with the details of the solvation term. For this purpose we have performed multicanonical simulations of polyalanine molecules of length 10. The protein-water interaction was included in two ways: either by a distance-dependent dielectric permittivity or by a term that is proportional to the solvent-accessible surface area of the peptide. For the latter case we have considered four different parameter sets: OONS (Ooi et al., 1987), JRF (Vila et al., 1991), W92 (Wesson and Eisenberg, 1992), and SCH (Schiffer et al., 1993). Quantities such as the energy, helicity, and susceptibility were calculated as functions of temperature. Our results were compared with that of gas-phase simulations. A strong dependence of the characteristics of the helix-coil transition from the details of the solvation term was found.

METHODS

Our investigation of the helix-coil transition for, and references therein polyalanine is based on a detailed, all-atom representation of that homopolymer. The interaction between the atoms was described by a standard force field, ECEPP/2 (Sippl et al., 1984) (as implemented in the program package SMMP; Eisenmenger et al., 2001), and is given by:

$$E_{\text{tot}} = E_{\text{C}} + E_{\text{LJ}} + E_{\text{HB}} + E_{\text{tor}}, \tag{1}$$

$$E_{\text{C}} = \sum_{(\text{i,j})} \frac{332 q_{\text{i}} q_{\text{j}}}{\varepsilon r_{\text{ij}}}, \tag{2}$$

$$E_{\text{LJ}} = \sum_{(\text{i,j})} \left(\frac{A_{\text{ij}}}{r_{\text{ij}}^{12}} - \frac{B_{\text{ij}}}{r_{\text{ij}}^{6}} \right), \tag{3}$$

$$E_{\text{HB}} = \sum_{(\text{i,j})} \left(\frac{C_{\text{ij}}}{r_{\text{ij}}^{12}} - \frac{D_{\text{ij}}}{r_{\text{ij}}^{10}} \right), \tag{4}$$

$$E_{\text{tor}} = \sum_{\text{l}} U_{\text{l}} (1 \pm \cos(n_{\text{l}} \chi_{\text{l}})), \tag{5}$$

Here, r_{ij} (in Å) is the distance between the atoms i and j, and χ_{l} is the lth torsion angle. We have chosen ECEPP/2 instead of the newer ECEPP/3 because this choice allows a more easy comparison with our previous work. Both force fields differ from each other only in the way in which prolines and endgroups are treated. In preliminary polyalanine simulations, we found no qualitative differences in our results when ECEPP/3 was used instead of ECEPP/2 (data not shown).

The interactions between our homo-oligomer and water are approximated by means of two implicit water models. In the first model (DDE) the electrostatic interactions in the presence of water rely on a distance dependent electrostatic permittivity (Hingerty et al., 1985):

$$\varepsilon(r) = D - \frac{D-2}{2} [(sr)^2 + 2sr + 2] e^{-sr}, \tag{6}$$

For the parameters D and s empirical values are chosen such that for large distances the permittivity takes the value of bulk water ($\varepsilon \approx 80$), and the value $\varepsilon = 2$ for short distances (protein interior space). Equation 6 is the result of interpolation of two types of interactions. For short distances it models the interaction of two charges placed in continuum medium, while

Submitted October 16, 2001 and accepted for publication December 24, 2001.

Address reprint requests to Dr. Ulrich H. E. Hansmann, 1400 Townsend Dr., Houghton, MI 49931-1295. Tel: 906-487-2909; Fax: 906-487-2933; E-mail: hansmann@mtu.edu.

0006-3495/02/06/3269/08 $2.00

over long distances it represents a Debye curve. This is clearly a gross oversimplification of protein-solvent interactions. However, approximating solvation effects by a distance-dependent dielectric permittivity was used by many authors to study the proteins and nucleic acids (e.g., (Laverty et al., 1986) because it does not significantly slow protein simulations below those of simple *in vacuo* simulations.

In another common approximation of the protein-solvent interaction, one assumes that the free energy contributions from atomic groups immersed in the protein interior differ from contributions of groups exposed to the water. It is commonly accepted (Ooi et al., 1987; Wesson 1992; Lee and Richards, 1971; Eisenberg and McLachlan, 1986) that this free-energy difference is proportional to the surface area of the atomic group exposed to the solvent. Within this approximation, the total solvation energy of a protein is given by the sum of contributions from each solvated atomic group:

$$E_{\mathrm{sol}} = \sum_{\mathrm{i}} \sigma_{\mathrm{i}} A_{\mathrm{i}}, \tag{7}$$

where E_{sol} is the solvation energy, A_{i} is the conformational dependent solvent accessible area of the surface of the *ith* atom, and σ_{i} is the atomic solvation parameter for the atom *i*. The summation is extended over all atomic groups. The solvation parameters are evaluated experimentally by measuring the free energy needed to bring the group from a nonpolar environment (usually octanol or ethanol are used as convenient compounds) into water. Many sets of solvation parameters were evaluated by several authors with different methods, but unfortunately it is not always obvious which one is the most appropriate. The sets we study here are named OONS (Ooi et al., 1987), JRF (Vila et al., 1991), W92 (Wesson and Eisenberg, 1992), and SCH (Schiffer et al., 1993), and are described in the respective references.

Simulations of detailed models of biological macromolecules are notoriously difficult. This is because the various competing interactions within the polymer lead to an energy landscape characterized by a multitude of local minima. Hence, in the low-temperature region, canonical Monte Carlo or molecular dynamics simulations will tend to get trapped in one of these minima and the simulation will not thermalize within the available CPU time. Only recently, with the introduction of new and sophisticated algorithms such as *multicanonical sampling* (Berg and Neuhaus, 1991) and other *generalized-ensemble* techniques (Hansmann and Okamoto, 1998) was it possible to alleviate this problem in protein simulations (Hansmann and Okamoto, 1993). For polyalanine, both the failure of standard Monte Carlo techniques and the superior performance of the multicanonical algorithm are extensively documented in earlier work (Okamoto and Hansmann, 1995). For this reason we again use this sophisticated simulation technique for our project. In the multicanonical algorithm (Berg and Neuhaus, 1991) conformations with energy E are assigned a weight $\omega_{\mathrm{mu}}(E) \gg 1/n(E)$. Here, $n(E)$ is the density of states. A simulation with this weight will lead to a uniform distribution of energy:

$$P_{\mathrm{mu}}(E) \propto n(E)\omega_{\mathrm{mu}}(E) = \mathrm{const}, \tag{8}$$

This is because the simulation generates a one-dimensional (1D) random walk in the energy space, allowing itself to escape from any local minimum. Because a large range of energies are sampled, one can use the reweighting techniques (Ferrenberg and Swendsen, 1988) to calculate thermodynamic quantities over a wide range of temperatures T by

$$\langle A\rangle_{\mathrm{T}} = \frac{\int dx A(x)\omega^{-1}(E(x))e^{-\beta \mathrm{E(x)}}}{\int dx \omega^{-1}(E(x))e^{-\beta \mathrm{E(x)}}}, \tag{9}$$

where x stands for configurations.

Unlike in the case of canonical simulations, the weights

$$\omega(E) = n^{-1}(E) = e^{-\mathrm{S(E)}}, \tag{10}$$

are not a priori known. Instead, estimators for these weights have to be determined. This is often done by an iterative procedure in which for reasons of numerical stability Eq. 10 is replaced by

$$\omega(E) = e^{-\beta(\mathrm{E})\mathrm{E}-\alpha(\mathrm{E})}, \tag{11}$$

The multicanonical parameters $\beta(E)$ and $\alpha(E)$ are defined through

$$\beta(E) = \frac{S(E') - S(E)}{E' - E}$$

and

$$\alpha(E) = \begin{cases} 0, & E \geq E_{\max} \\ \alpha(E') + (\beta(E') - \beta(E))E', & E < E_{\max} \end{cases} \tag{12}$$

with E and E' adjacent bins in the array $S(E)$. The $\beta(E)$ are then iteratively updated (Berg, 1996) by the relation

$$\beta^{\mathrm{i}+1}(E) = \beta^{\mathrm{i}}(E) + g_0(E) \cdot (\ln H^{\mathrm{i}}(E') - \ln H^{\mathrm{i}}(E))/(E' - E), \tag{13}$$

in which $H^{\mathrm{i}}(E)$ is the histogram of the ith run (and $H(E) \geq 1$). In Berg (1996) the factor $g_0(E)$ in Eq. 13 was defined through

$$g_0(E) = \frac{\hat{g}^{\mathrm{i}}(E)}{\hat{g}^{\mathrm{i}}(E) + \sum_{\mathrm{j}}^{\mathrm{i}-1} \hat{g}^{\mathrm{j}}(E)}$$

with

$$g^{\mathrm{i}}(E) = \frac{H^{\mathrm{i}}(E') \cdot H^{\mathrm{i}}(E)}{H^{\mathrm{i}}(E') - H^{\mathrm{i}}(E)}. \tag{14}$$

The above relation assumes that the histogram $H(E)$ counts independent events, which is in general not true. Hence, it is more appropriate and leads to a faster convergence of $\beta(E)$ if the array $\hat{g}^{\mathrm{i}}(E)$ in Eq. 14 is instead defined by

$$\hat{g}^{\mathrm{i}}(E) = \frac{K^{\mathrm{i}}(E')K^{\mathrm{i}}(E)}{K^{\mathrm{i}}(E') + K^{\mathrm{i}}(E)}, \tag{15}$$

where the auxiliary array $K(E)$ now counts only the number of *independent* visits at energy E.

With the above-described iterative procedure, we needed 200,000 sweeps for the weight factor calculations. All thermodynamic quantities were then estimated from one production run of 1,000,000 Monte Carlo sweeps starting from a random initial conformation, i.e., without introducing any bias.

RESULTS AND DISCUSSION

In previous gas-phase simulations of polyalanine (Hansmann and Okamoto, 1999; Alves and Hansmann, 2000, 2001; Okamoto and Hansmann, 1995) we observed at $T = 430\ K$ a pronounced transition between a high-temperature phase dominated by disordered coil structures and an ordered phase with single, extended helices. A natural order parameter for this helix-coil transition is the average num-

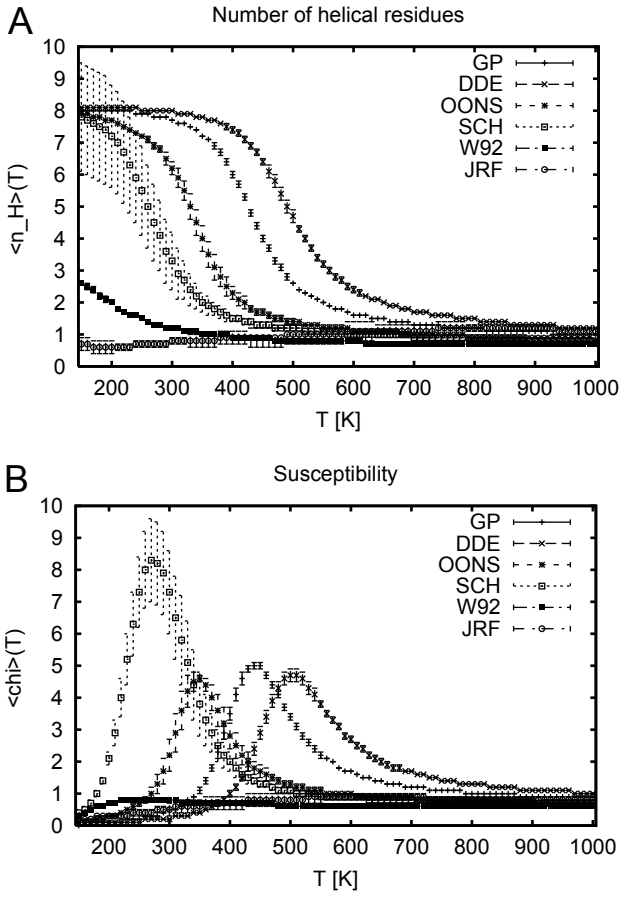

FIGURE 1 Temperature dependence of (*A*) the average number $\langle n_H \rangle$ of helical residues and (*B*) the susceptibility $\chi(T)$ for ALA_{10} as calculated from a gas-phase simulation and from simulations with various solvation energy terms. All results rely on multicanonical simulations of 1,000,000 Monte Carlo sweeps each.

ber $\langle n_H(T) \rangle$ of residues in the oligomer that are part of an α-helix. Following earlier work (Okamoto and Hansmann, 1995) we define a residue as helical if the pair of backbone dihedral angles ϕ, ψ takes a value in the range (-70 ± 20, -37 ± 20). In Fig. 1*A* this order parameter is displayed as function of temperature for a gas-phase simulation (GP) of Ala_{10} and simulations with the various solvation terms. Fig. 1 *B* shows the corresponding plots for the susceptibility $\chi(T)$ defined by

$$\langle \chi(T) = \langle n_H^2(T) \rangle - \langle n_H(T) \rangle^2, \qquad (16)$$

In Fig. 1, *A* and *B*, the curves representing the various simulations fall into three groups. For the case where the protein-solvent interaction was approximated by a distance-dependent permittivity (DDE), both $\langle n_H \rangle$ and χ have a similar temperature dependence than is observed for polyalanine in gas-phase simulations (GP). However, the transition temperature T_c is shifted from $T = 435 \pm 20$ K (gas-phase) to a *higher* value $T = 495 \pm 20$. This temperature was determined from the maximum of the susceptibility $\chi(T)$ in Fig. 1 *B* and is listed in Table 1. To the same group belong the simulations in which the solvation energy was approximated by a solvent-accessible surface term with either the OONS (Ooi et al., 1987) or SCH (Schiffer et al., 1993) parameter set. In both cases susceptibility χ and order parameter $\langle n_H(T) \rangle$ show a temperature dependence similar to the one of gas-phase simulations. Only now, the transition temperature T_c is shifted to *lower* temperatures. The corresponding transition temperatures can again be determined from the positions of the maximum in $\chi(T)$ and are listed in Table 1. The shift toward lower temperatures was one of the main results reported in Mitsutake and Okamoto (1999, 2000) for simulations with the OONS solvation energy, and our $T_c = 345 \pm 20$ K agrees well with their value, $T_c = 340$ K (no errors quoted).

TABLE 1 Transition temperatures for the helix-coil transition in Ala_{10} as obtained from gas-phase simulations and simulations with various solvent representations

Model	T_c
GP	435 (20)
DDE	495 (20)
OONS	345 (15)
SCH	285 (25)
W92	—
JRF	—

All results rely on multicanonical simulations of 1,000,000 Monte Carlo sweeps each.
The numbers in parentheses are the standard deviations of the respective quantities.

A somehow different behavior is observed in the simulation where the protein-water interaction was approximated by a solvent-accessible surface term relying on the W92 (Wesson and Eisenberg, 1992) parameter set. Here, the form of $\langle n_H \rangle$ indicates only partial helix formation and occurs only at much lower temperatures. The susceptibility $\chi(T)$ in Fig. 1 *B* gives no indication for a helix-coil transition. For this reason, no value of T_c is listed for the W92 parameter set in Table 1. Instead, we observe in Fig. 2 for this case at low temperatures even the appearance of residues whose backbone dihedral angles ϕ, ψ take values typical for a β-sheet (-150 ± 30, 150 ± 30).

Yet another behavior is observed in simulations where the solvation energy of Eq. 7 is evaluated by means of the JRF parameter set (Vila et al., 1991). No formation of helices or sheets is observed in Figs. 1 and 2. Because no transition temperature can be determined, we do not list a value of T_c for the JRF parameter set in Table 1.

The same grouping can be found in Fig. 3, *A–F*, where we display various energy terms as a function of temperature. In these figures we have shifted the solvation energies and the partial ECEPP/2 energies E_C, E_{LJ}, E_{HB}, and E_{tor} of Eq. 5 by a constant term such that we have for all solvation models at $T = 1000$ K, $E_{sol} = 0$ and $E_C = E_{LJ} = E_{HB} = E_{tor} = 0$. Such a shift by an irrelevant constant allows a better

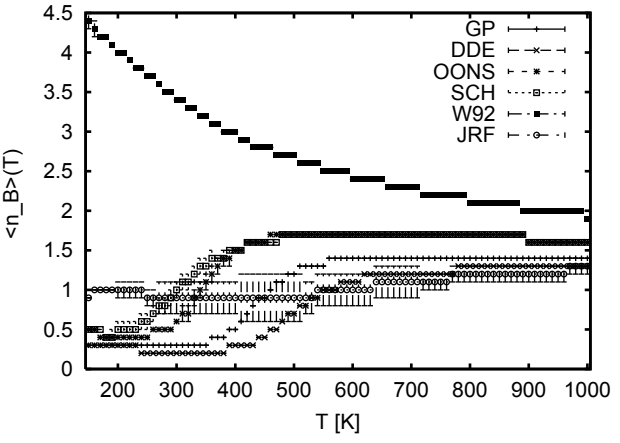

FIGURE 2 Temperature dependence of the average number $\langle n_B \rangle$ of residues whose backbone dihedral angles ϕ, ψ take values as typically found in β-sheets. Results from a gas-phase simulation and such with various solvation terms are presented for ALA_{10}. All data rely on multicanonical simulations of 1,000,000 Monte Carlo sweeps.

comparison of the different simulations. The average total energy $\langle E_{tol} \rangle$, which is the sum of intramolecular potential energy $E_{ECEEP/2}$ and the solvation energy E_{sol}, is displayed in Fig. 3 *A*. We observe again that simulations with the parameter sets OONS and SCH, and such with distant dependent permittivity (DDE), have temperature dependence similar to GP simulations. However, in simulations relying on the W92 parameter set, the energy varies less with temperature and is considerably higher than in the simulations with other solvation energy terms at low temperatures. Finally, the energy in simulations with the JRF parameter set is an almost linear function of temperature and is much lower than the energies found in gas phase simulations, especially at high temperatures.

The dissimilar behavior of energy for simulations with different solvation terms is even more obvious in Fig. 3 *B*, where the average intramolecular energy $E_{ECEPP/2}$ is drawn. While this energy term decreases between 1000 K and 150 K by ≈50 kcal/mol (with most of that change, ≈30 kcal/mol, happening around the respective transition temperature, T_c) in GP simulations and in simulations with OONS, SCH, and DDE solvation terms, it changes in the same temperature interval only by ≈20 kcal/mol in simulations utilizing the JRF or W92 parameter sets. Because for these two parameter sets no or little helix formation was observed, it seems likely that the formation of helices is related to the large gain in potential energy observed for GP, OONS, SCH, and DDE simulations. This gain in potential energy is in part due to the formation of hydrogen bonds between a residue and the fourth following one in the polypeptide chain that stabilize an α-helix. Fig. 3 *C* displays the average hydrogen-bonding energy $\langle E_{HB} \rangle$ of Eq. 5 as a function of temperature, and one can clearly see the gain in energy for the GP, DDE, OONS, and SCH simulations at the respective helix-coil transition temperatures of Table 1. No such gain is observed in W92 and JRF simulations, where also no helix formation was found. A similar gain in energy with helix formations in gas-phase and simulations with DDE, OONS, and SCH solvent representations is also observed for the average Lennard-Jones energy $\langle E_{LJ} \rangle$ and the electrostatic energy $\langle E_C \rangle$ displayed in Fig. 3, *D* and *E*, respectively. Note also in Fig. 3 *E* the large gain in E_C for DDE at the helix-coil transition temperature, which additionally stabilizes the α-helix in this model.

A complementary picture is found in Fig. 3 *F*, where the solvation energy E_{sol} is shown as a function of temperature. The observed helix formation in gas-phase simulations and such with OONS, SCH, and DDE solvent representations is correlated with an increases of the solvation energies by ≈5 kcal/mol. However, in simulations with the W92 and JRF parameter sets, for which no helix-formation was observed in Fig. 1, E_{sol} decreases with temperature. This decrease is only ≈5 kcal/mol for W92, but it is much larger (on the order of 30 kcal/mol) in the case of JRF, where the solvation energy is the dominant term.

The effects of the dominant solvation term in simulations with the JRF parameter set can also be seen in Fig. 4. In this figure the average radius of gyration, a measure for the compactness of configurations, is shown as a function temperature. One can see that this quantity changes little with temperature for the JRF data. However, its value is over the whole temperature range considerably smaller than observed in the other simulations. This indicates that the JRF solvation term favors compact configurations at high temperatures, and that the pressure toward compact structure is such that the more elongated helices cannot be formed. Note, however, that the tendency toward compact configurations does not lead to a lower Lennard-Jones energy E_{LJ}, as one would expect. Fig. 3 *D* indicates that $\langle E_{LJ} \rangle$ is, at low temperatures in JRF simulations, even larger than in GP, DDE, OONS, and SCG simulations where helix-formation was observed. The tendency toward compact structures in JRF simulations may be due to the fact that the JRF parameter set was developed from minimum energy (i.e., compact) conformations of peptides (the low-energy conformations of 13 tetrapeptides derived by NMR studies (Vila et al., 1991)), and therefore this parameter set may have an intrinsic bias toward compact structures.

However, the W92 parameter set was developed from measurements of free energies of amino acid side chain analogs from vapor to water (Wolfenden et al., 1981). The parameters for this set are negative for all atoms except carbon, meaning that the nitrogen, oxygen, and sulfur atoms are considered hydrophilic, i.e., favoring solvent exposure. This explains not only the small solvation energies observed for this parameter set in Fig. 3 *F*, but also why in Fig. 4 the radius of gyration is consistently larger for this parameter set than for the others, indicating that extended configura-

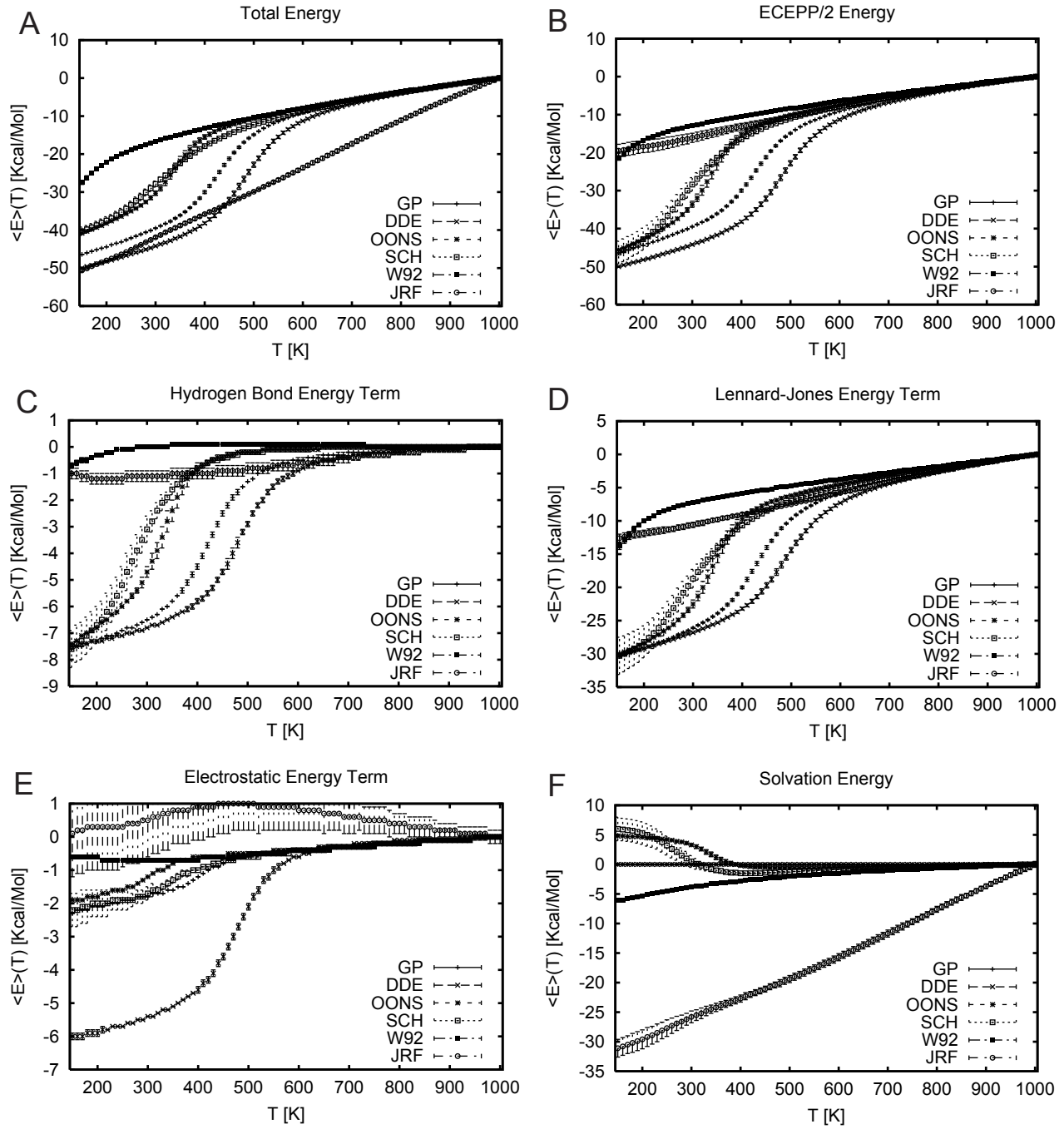

FIGURE 3 Temperature dependence of (*A*) the total energy $\langle E_{\text{total}} = E_{\text{ECEPP/2}} + E_{\text{sol}} \rangle$, (*B*) the intramolecular energy $\langle E_{\text{ECEPP/2}} \rangle$, (*C*) the hydrogen-bonding energy $\langle E_{\text{HB}} \rangle$, (*D*) Lennard-Jones energy $\langle E_{\text{LJ}} \rangle$, (*E*) Coulomb energy $\langle E_{\text{C}} \rangle$, and (*F*) the solvation energy $\langle E_{\text{sol}} \rangle$ as calculated from a gas-phase simulation and from simulations with various solvation energy terms. All results rely on multicanonical simulations of ALA_{10} with 1,000,000 Monte Carlo sweeps for each case.

tions are favored with this parameter set. This bias toward extended structures again limits the formation of α-helices.

While the OONS parameter set was derived from experimental free energies of gas-to-water transfer of small aliphatic and aromatic molecules, the SCH parameter set is not directly based on experimental free energy data. Instead, it was developed as an optimized parameter set to complement the CHARMM force field (Brooks et al., 1983). In both parameter sets the hydrophobic character of the carbon atoms is increased and the hydrophilic character of uncharged oxygen and nitrogen atoms decreased, resulting in the large solvation energies of these two parameter sets

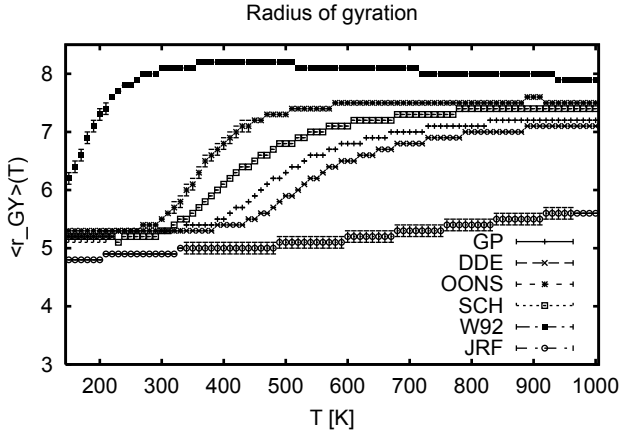

FIGURE 4 Temperature dependence of the average radius-of-gyration $\langle R_{gy} \rangle$ as measured in gas-phase simulations and simulations with various solvent representations. All data rely on multicanonical simulations of 1,000,000 Monte Carlo sweeps.

(when compared with the one of the W92 parameter set) that one observes in Fig. 3 *F*. The OONS and SCH solvation energies again favor extended structures (the radius of gyration has larger values than found in gas-phase simulations); however, the interplay of solvation energies and intramolecular ECEPP/2 energy is such that the radius of gyrations (and consequently the compactness) of polyalanine configurations as a function of temperature shows behavior similar to the gas-phase simulation. The same is true for the DDE simulation, where the protein-solvent interaction was approximated by a distance-dependent permittivity.

Our results demonstrate that the helix formation is due to the gain in potential (intramolecular) energy while (with the exception of the JRF parameter set) the solvent-accessible surface terms favor extended peptide configurations. Table 2 summarizes the differences in total energy ΔE_{tot}, solvation energy ΔE_{sol}, potential energy $\Delta E_{ECEEP/2}$, and the partial energies. ΔE_C, ΔE_{LJ}, ΔE_{HB}, and ΔE_{tor} between complete helical configurations (all residues with exception of the terminal ones are part of an α-helix) and coil configurations at temperature $T = 300$ K for gas-phase, DDE, OONS, and SCH simulations. Note that the intramolecular energy differences $\Delta E_{ECEEP/2}$ of gas-phase, OONS, and SCH simulations have the same values within their error bars. For simulations with the W92 parameter set the longest found helix consists of six consecutive residues. Hence, for this case we measured only the energy difference between configurations with at least three consecutive helical-residues (i.e., one turn of an α-helix) and coil configurations. This modified definition of the energy differences is also the reason for the smaller value of $\Delta E_{ECEEP/2}$ listed for W92 in Table 2. We do not list energy differences for the JRF parameter set because no helices were found in simulations utilizing this parameter set.

Note that in simulations with distant dependent permittivity (DDE), helices are energetically more favored than in the gas-phase simulations. This is due to the increased contribution from the Coulomb term E_C, as one can also see in Fig. 3 *E*. The larger energy gap between helical and coil conformations (when compared with gas-phase simulations) explains why the transition temperature is higher in DDE simulations than in gas-phase simulations.

For the OONS and SCH parameter set the solvation energy difference ΔE_{sol} is positive (indicating that coil structures are energetically favored), but its magnitude is only approximately half that of the potential energy difference $\Delta E_{ECEEP/2}$. Hence, there is still an overall energetic gain connected with helix formation. However, in both cases the total energy difference between helical and coil configurations is reduced by the solvation energy when compared with the gas-phase simulation. This reduction of the energy gap leads to the lower transition temperatures observed in OONS and SCH simulations.

However, for the W92 parameter set we find that $\Delta E_{ECCP/2}$ and ΔE_{sol} are of some magnitude, so that helical configurations are not or only weakly energetically favored. This is consistent with our results in Fig. 1, *A* and *B*, where we find at $T = 280$ K a high average helicity in OONS and SCH simulations, but only a small value of $\langle n_H \rangle$ and no indications for a helix-coil transition in W92 simulations. An evaluation of energy differences was not possible for simulations with the JRF parameter set because no helices were found.

The above results indicate that the existence and characteristics of the helix-coil transition in polyalanine strongly depend on the details of the solvent representation. To

TABLE 2 Energy differences between helical and configurations (see text) at $T = 280$ K as measured in gas-phase simulations and simulations with various solvent representations

Model	ΔE_{tol}	ΔE_{sol}	$\Delta E_{ECEPP/2}$	ΔE_C	ΔE_{LJ}	ΔE_{HB}	ΔE_{or}
GP	−16.9 (1)	—	−16.9 (1)	0.4 (3)	−12.1 (1)	−4.3 (3)	−0.8 (1)
DDE	−17.9 (6)	—	−17.9 (6)	−3.6 (2)	−10.1 (4)	−3.9 (2)	−0.3 (1)
OONS	−11.3 (9)	4.1 (3)	−15.4 (6)	−0.2 (1)	−10.7 (4)	−4.1 (1)	−0.4 (1)
SCH	−7.1 (5)	8.7 (1)	−15.8 (5)	0.7 (3)	−11.2 (2)	−4.6 (3)	−0.7 (1)
W92	−0.7 (7)	5.6 (6)	−6.3 (1.1)	0.8 (1)	−5.8 (9)	−1.0 (2)	−0.3 (1)
JRF	—	—	—	—	—	—	—

All results rely on multicanonical simulations of 1,000,000 Monte Carlo sweeps of Ala_{10} for each case.
The numbers in parentheses are the standard deviations of the respective quantities.

TABLE 3 Helix propagation parameter s and nucleation parameter σ at $T = 280$ K for Ala_{10} as measured in gas-phase simulations and simulations with various solvent representations

Model	s	σ
GP	1.67 (9)	0.15 (1)
DDE	1.78 (12)	0.15 (1)
OONS	1.31 (15)	0.13 (1)
SCH	1.02 (15)	0.11 (2)
W92	≈ 0	>1
JRF	≈ 0	>1

All results rely on multicanonical simulations of 1,000,000 Monte Carlo sweeps for each case.
The numbers in parentheses are the standard deviations of the respective quantities.

evaluate the validity of the different solvent models one has to compare the numerical results with experimental data. For this purpose we have calculated the helix propagation parameter s, which was also determined by experiments (Wojcik et al., 1990; Chakrabartty and Baldwin, 1993). According to the Zimm-Bragg model (Zimm and Bragg, 1959) the average number of helical residues $\langle n \rangle$ and the average length $\langle l \rangle$ of a helical segment are given for a large number of residues N by

$$\frac{\langle n \rangle}{N} = \frac{1}{2} - \frac{1 - s}{2\sqrt{(1 - s)^2 + 4s\sigma}}, \tag{17}$$

$$\langle l \rangle = 1 + \frac{2s}{1 - s + \sqrt{(1 - s)^2 + 4s\sigma}}, \tag{18}$$

where s is the helix propagation parameter and σ the nucleation parameter of the Zimm-Bragg model. From these equations with the values of $\langle n \rangle / N$ and $\langle l \rangle$ calculated from the multicanonical production runs, we have calculated s at temperature $T = 280$ K for gas-phase and the different solvation models. Our values are summarized in Table 3, which also lists our σ values. Our results for gas-phase, DDE, and OONS simulations are in agreement with the experimental results of Charabartty and Baldwin (1993) where they list values of s(Ala) between 1.5 and 2.19. However, the s value obtained in the SCH simulation agrees well with the one obtained by the host-guest technique of Wojcik et al. (1990). However, the s values, which were obtained in W92 or JRF simulations, do not agree with either of the experimental data. Hence, we conclude that the W92 and JRF parameter sets are not appropriate solvation models in simulations of polyalanine. Otherwise, the variation in the experimental data is too large to give indications whether one of the remaining solvent representations (DDE, OONS, SCH, or even no solvent at all (GP)) is preferable over the others.

CONCLUSIONS

We have performed multicanonical simulations of polyalanine. The intramolecular forces were modeled by the ECEPP/2 force field, and various approximations for the solvation energy were studied. We observed that whether a helix-coil transition is observed for polyalanine, and at what temperature, depends strongly on the chosen approximation for the protein-solvent interaction. Our results demonstrate both the importance (and need) of including solvation terms into protein simulations and the difficulties in choosing an adequate representation of the protein-water interactions. Especially when using the solvent-accessible surface approach, it seems necessary to carefully choose a parameter set that is suitable for the problem under consideration. Use of a specific parameter set without further justification could otherwise generate misleading results.

This article was written in part while U.H. was a visitor at the Department of Physics at University of Central Florida. He thanks Alfons Schulte, Weili Luo, Aniket Bhattacharya, and Brian Tonner for their kind hospitality during his stay in Orlando.

This work was supported in part by National Science Foundation Grant CHE-9981874 (to U.H.).

REFERENCES

Alves, N. A., and U. H. E. Hansmann. 2000. Partition function zeros and finite size scaling of helix-coil transitions in a polypeptide. *Phys. Rev. Lett.* 84:1836–1839.

Alves, N. A., and U. H. E. Hansmann. 2001. Yang-Lee zeros and the helix-coil transition in a continuum model of polyalanine. *Physica A.* 292:509–518.

Berg, B. A. 1996. Multicanonical recursions. *J. Stat. Phys.* 82:323–342.

Berg, B. A., and T. Neuhaus. 1991. Multicanonical algorithms for first-order phase transitions. *Phys. Lett. B.* 267:249–253.

Brooks, B. R., R. E., Bruccolieri, B. D., Olafson, D. J., States, S., Swaminathan, and M. Karplus. 1983. CHARMM: a program for macromolecular energy, minimization, and dynamics calculations. *J. Comp. Chem.* 4:187–217.

Chakrabartty, A., and R. L. Baldwin. 1993. *Protein Folding: In Vivo and In Vitro.* J. Cleland and J. King, editors. ACS Press, Washington, D.C. 166–177.

Eisenberg, D., and A. D. McLachlan. 1986. Solvation energy in protein folding and binding. *Nature.* 319:199–203.

Eisenmenger, F., U. H. E., Hansmann, Sh., Hayryan, and C. K. Hu. 2001. SMMP: a modern package for simulation of proteins. *Comp. Phys. Comm.* 138:192–212.

Ferrenberg, A. M., and R. H. Swendsen. 1988. New Monte Carlo technique for studying phase transitions. *Phys. Rev. Lett.* 61:2635–2638.

Hansmann, U. H. E., and Y. Okamoto. 1993. Prediction of peptide conformation by multicanonical algorithm: a new approach to the multiple-minima problem. *J. Comp. Chem.* 14: 1333–1338.

Hansmann, U. H. E., and Y. Okamoto. 1998. The generalized-ensemble approach for protein folding simulations. *In Annual Reviews in Computational Physics. VI.* D. Stauffer, editor. World Scientific, Singapore. 129–157.

Hansmann, U. H. E., and Y. Okamoto. 1999. Finite-size scaling of helix-coil transitions in polyalanine studied by multicanonical simulations. *J. Chem. Phys.* 110:1267–1276; 111:1339(erratum).

Hingerty, B., R. H., Richie, T. L., Ferrel, and J. Turner. 1985. Dielectric effects in biopolymers: the theory of ionic saturation revisited. *Biopolymers.* 24:427–439.

Hudgins, R. R., M. A., Ratner, and M. F. Jarrold. 1998. Design of helices that are stable in vacuo. *J. Am. Chem. Soc.* 120:12974–12975.

Kemp, J. P., and Z. Y. Chen. 1998. Formation of helical states in wormlike polymer chains. *Phys. Rev. Lett.* 81:3880–3883.

Lavery, R., H. Sklenar, K. Zakrzewska, and B. Pullman. 1986. The flexibility of the nucleic acids. II. The calculation of internal energy and applications to mononucleotide repeat DNA. *J. Biomol. Struct. & Dyn.* 3:989–1014.

Lee, B., and F. M. Richards. 1971. Interpretation of protein structures: estimation of static accessibility. *J. Mol. Biol.* 55:379–400.

Mitsutake, A., and Y. Okamoto. 1999. α-Helix propensities of homo-oligomers in aqueous solution by multicanonical algorithm. *Chem. Phys. Lett.* 309:95–100.

Mitsutake, A., and Y. Okamoto. 2000. Helix-coil transitions of amino acid homo-oligomers in aqueous solution studied by multicanonical simulations. *J. Chem. Phys.* 112:10638–10647.

Okamoto, Y., and U. H. E. Hansmann. 1995. Thermodynamics of helix-coil transitions studied by multicanonical algorithms. *J. Phys. Chem.* 99:11276–11287.

Ooi, T., M., Obatake, G., Nemethy, and H. A. Scheraga. 1987. Accessible surface areas as a measure of the thermodynamic parameters of hydration of peptides. *Proc. Natl. Acad. Sci. U.S.A.* 8:3086–3090.

Poland, D., and H. A. Scheraga. 1970. *Theory of Helix-Coil Transitions in Biopolymers.* Academic Press, New York.

Schiffer, C. A., J. W., Caldwell, P. A., Kollman, and R. M. Stroud. 1993. Protein structure prediction with a combined solvation free energy molecular mechanics force field. *Mol. Simul.* 10:121–149.

Sippl, M. J., G., Némethy, and H. A. Scheraga. 1984. Intermolecular potentials from crystal data. 6. Determination of empirical potentials for O–H ··· O=C hydrogen bonds from packing configuration. *J. Phys. Chem.* 88:6231–6233.

Vila, J., R. L., Williams, M., Vásquez, and H. A. Scheraga. 1991. Empirical solvation models can be used to differentiate native from near-native conformations of bovine pancreatic trypsin inhibitor. *Proteins: Struct, Funct, Genet.* 10:199–218.

Wesson, M., and D. Eisenberg. 1992. Atomic solvation parameters applied to molecular dynamics of proteins in solution. *Protein Sci.* 1:227–235.

Wojcik, J., K. H. Altmann, and H. A. Scheraga. 1990. Helix-coil stability constants for the naturally-occurring amino-acids in water. 24. Half-cystine parameters from random poly(hydroxibutylglutamine CO-S-methylthiol-L-cystine). *Biopolymers*. 30:121–134.

Wolfenden, R., L., Andersson, P. M., Cullis, and C. C. B. Southgate. 1981. Affinities of amino acid side chains for solvent water. *Biochemistry.* 20:849–855.

Zimm B. H., and J. K. Bragg. 1959. Theory of the phase transition between helix and random coil in polypeptide chains. *J. Chem. Phys.* 31: 526–535.